

# Boron Nitride Monolayer: A Strain Tunable Nanosensor

M. Neek-Amal,<sup>\*,†,‡</sup> J. Beheshtian,<sup>†,‡</sup> A. Sadeghi,<sup>†</sup> K. H. Michel,<sup>†</sup> and F. M.  
Peeters<sup>†</sup>

*Departement Fysica, Universiteit Antwerpen, Groenenborgerlaan 171, B-2020 Antwerpen,  
Belgium, and Department of Physics, Shahid Rajaee Teacher Training University, Lavizan,  
Tehran 16785-136, Iran*

E-mail: neekamal@srttu.edu, (Tel: +3232653661)

---

<sup>\*</sup>To whom correspondence should be addressed

<sup>†</sup>Universiteit Antwerpen

<sup>‡</sup>Shahid Rajaee Teacher Training University

## **Abstract**

The influence of triaxial in-plane strain on the electronic properties of a hexagonal boron-nitride sheet is investigated using density functional theory. Different from graphene, the tri-axial strain localizes the molecular orbitals of the boron-nitride flake in its center depending on the direction of the applied strain. The proposed technique for localizing the molecular orbitals that are close to the Fermi level in the center of boron nitride flakes can be used to actualize engineered nanosensors, for instance, to selectively detect gas molecules. We show that the central part of the strained flake adsorbs polar molecules more strongly as compared to an unstrained sheet.

**Keywords:** hexagonal Boron-Nitride flake, piezoelectricity, localized states, Nanosensor

# Introduction

Strain engineering can be used to control the electronic properties of nanomaterials. This is of interest for fundamental physics, but is also relevant for potential device applications in nanoelectronics. Because the electronic and mechanical properties of an atomic monolayer are strongly influenced by strain they have attracted considerable attention over the last decades.<sup>1,2</sup>

Unlike graphene, a h-BN sheet is a wide gap insulator, as is bulk h-BN, and is a promising material for opto-electronic technologies,<sup>3-5</sup> tunnel devices and field-effect transistors.<sup>6</sup> Using a combination of mechanical exfoliation and reactive ion etching, monolayer and multilayer suspended h-BN sheets can be prepared.<sup>7</sup> The band gap of boron nitride nanoribbons can be altered by edge passivation with different types of atoms.<sup>8-10</sup>

A combination of an odd number of h-BN layers is a non-centrosymmetric ionic crystal which is piezoelectric due to  $D_{3h}$  symmetry.<sup>11,12</sup> The corrugations on the h-BN sheet results in a strong polarization in the plane of the sheet which depends non-analytically on the wave vector of the corrugations.<sup>13</sup> h-BN sheet has a non-linear elastic deformation up to an ultimate strength followed by a strain softening to failure.<sup>14,15</sup> Moreover, the band gap of boron nitride nanotubes can be reduced by a transverse electric field due to a mixing of states within the highest occupied molecular orbital and the lowest unoccupied molecular orbital.<sup>16-19</sup> The reduction in the band gap due to uniaxial strain results in tunneling magnetoresistance ratio which increases linearly with applied strain.<sup>20</sup> Here we propose an alternative approach for electron hole localization based on a tunable parameter, i.e. inhomogeneous strain.

Developments of nanosensors of (different) gases is to a great extent related to the response to both the morphology and the surface states of the material. Single-wall carbon nanotubes (SWNT) can act as a chemical sensor for sensing gaseous molecules such as  $\text{NO}_2$  or  $\text{NH}_3$  where the electrical resistance of a semiconducting SWNT is found to dramatically increase or decrease.<sup>21-24</sup> Here we study the effect of strain on the adsorption mechanism and propose a new and tunable way to control the adsorption of a gas.

In this paper, using density functional theory (DFT) calculations, we show a spatial separa-

tion of the highest occupied and lowest unoccupied molecular orbitals (i.e. HOMO and LUMO) in response to a triaxial in-plane strain. The result is in agreement with the predictions from piezoelectricity theory. Consequently, the binding energy of an external polar molecule over the strained sample is considerably enhanced. Depending on the applied triaxial strain on the zig-zag edges with boron (nitrogen) termination the HOMO (LUMO) is confined in the central portion of the flake. This study opens a new avenue in the field of strain engineering of a monolayer of h-BN in terms of tunable spatial localization of the frontier orbitals. (it controls and enhances chemical reaction). In recent experiments the edge structure of graphitic nanostructures were successfully controlled<sup>25</sup> and well defined (e.g. hexagonal shape) graphene flakes with zig-zag edges were observed.<sup>26</sup> Consequently, the proposed experimental set up is realistic and therefore we expect that the calculated effects will be measurable on micron size samples employing experimental realized controlled edge chirality.<sup>25-27</sup> A simple experimental set up for creating triaxial strain was proposed in Ref.<sup>2</sup>

The paper is organized as follows. In Sec. II, we present our theoretical approach for triaxial strain and corresponding piezoelectricity. In Sec. III we present the molecular dynamics simulation and density functional calculation methods. Then in Sec. IV we give and discuss our results. We conclude the paper in Sec. V.

## Theoretical Model

1(a) shows a hexagonal h-BN flake with zig-zag edges passivated by hydrogen. The distortion of a hexagonal boron-nitride flake subjected to triaxial strain along three equivalent crystallographic directions is shown schematically in 1(b). The original shape is shown by the dotted-red circles and the deformed shape by the blue-solid curves. In polar coordinates  $(r, \theta)$  the applied triaxial strain results in a displacement vector<sup>2</sup>  $u = (u_r, u_\theta) = C r^2 (\sin(3\theta), \cos(3\theta))$ , where  $C$  is a constant determining the strength of the applied strain and has dimension of inverse length. Notice that the  $r^2$ -dependence in  $u$  insures that the applied triaxial strain can also be realized on an infinite or

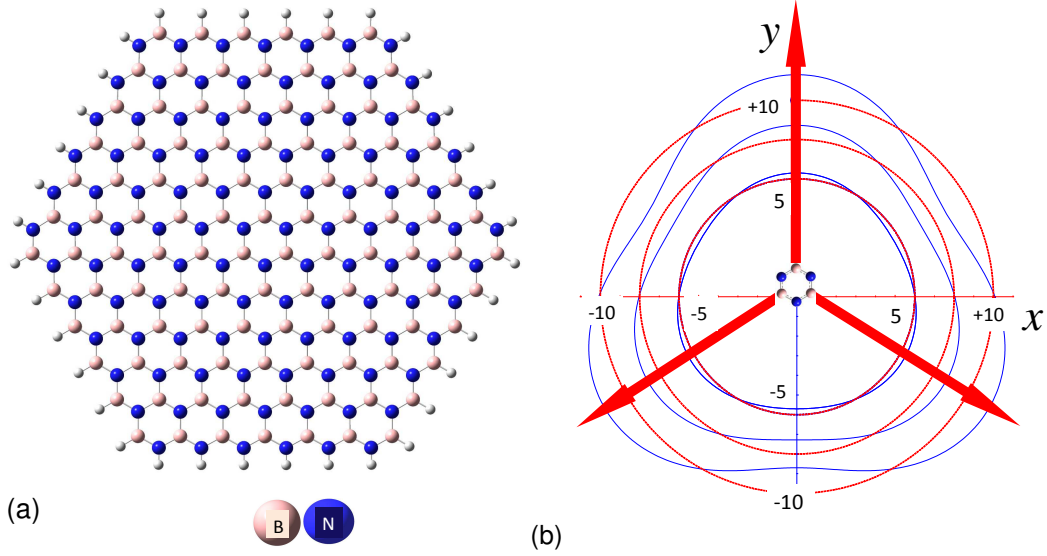


Figure 1: (a) Hexagonal flake of BN passivated by H atoms (white balls). (b) A schematic representation of the distorted hexagonal boron nitride flake by the applied triaxial strain. The red curves represent the original shape and the blue curves indicate the distorted flake. The flake is stretched along the three crystallographic directions which are represented by the three red vectors. The NB system is obtained by interchanging B and N atoms, or equivalently by rotating (a) and the central hexagon in (b) by an angle  $\pi/3$ , see 3(d,e,f).

macroscopic sheet. In the following we will first present a simple analytical theory that agrees qualitatively with our numerical DFT results.

Linear elasticity theory for an isotropic material leads to the stress-strain relation, i.e.  $\sigma_{jk} = \lambda \delta_{jk} \nabla \cdot u + 2\mu \varepsilon_{jk}$ , where  $\lambda$  and  $\mu$  are the Lamé parameters that determine the stiffness of the material. If we substitute  $u$  in the latter equation the components of the stress tensor in polar coordinates are written as

$$\sigma(r, \theta) = 4\mu C r \begin{pmatrix} \sin(3\theta) & \cos(3\theta) \\ \cos(3\theta) & -\sin(3\theta) \end{pmatrix}.$$

Here, it is more convenient to use the components of the stress tensor in Cartesian coordinates where the y axis is taken along the arm-chair direction and the x axis is taken along the zig-zag direction. The edges under strain can have B (called BN system) or N (called NB system) atoms (e.g. in 1(a), the strain is applied on B atom edges, i.e. the BN system is stretched along the red arrows). Note that the three strained edges (or free edges) have only one type of atoms. We

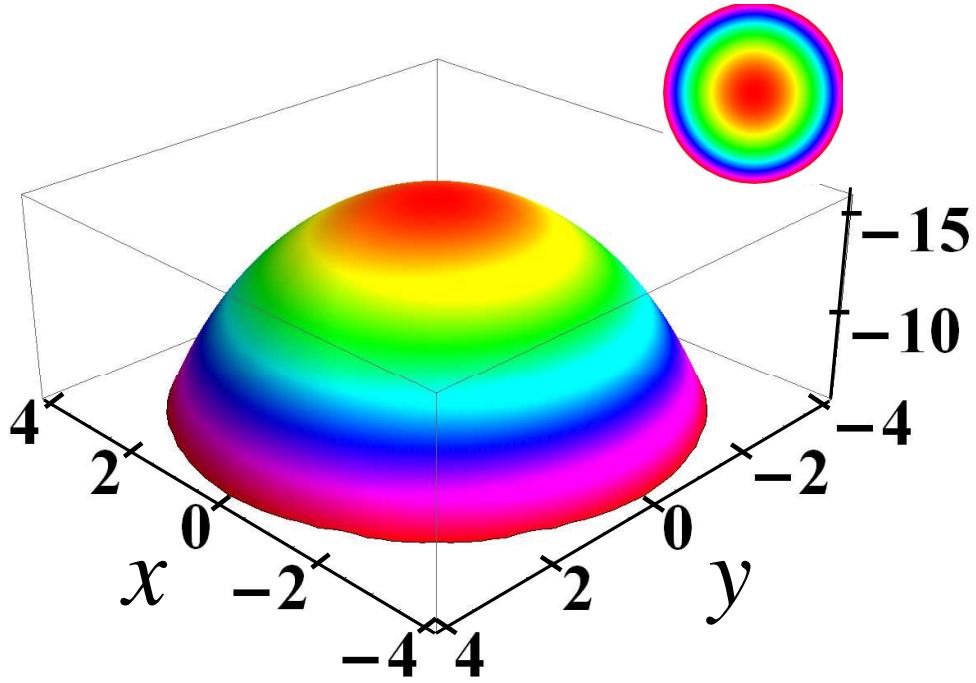


Figure 2: Electrostatic potential in arbitrary units at distance  $z = 2 \times 10^{-4}R$  above a disk of radius  $R$  subject to triaxial strain as predicted by our theoretical model based on linear theory of piezoelectricity (inset shows top view).

consider here the case of strained B edges, i.e. the BN flake of 1.

Using the product  $\sigma(x, y) = \Re \sigma(r, \theta) \Re^T$ , where  $\Re$  is the rotation matrix about the  $z$  axis, the stress tensor in Cartesian coordinates can be rewritten as

$$\sigma(x, y) = 4\mu C \begin{pmatrix} y & x \\ x & -y \end{pmatrix}.$$

On the other hand, an elastic in-plane deformation of the h-BN flake lowers its lattice symmetry, redistributes the valance charges in terms of shifting  $\sigma$  and  $\pi$  bonds and produces a non-zero polarization. Using linear piezoelectricity theory, the induced polarization due to the applied strain can be written as  $P_i = d_{i,jk} \sigma_{jk}$ , where  $d$  is the third rank piezoelectricity tensor which has in general (in two dimensions) 8 elements where the indices  $(i, j, k)$  can be  $x$  and  $y$ . The  $3m$  symmetry of the h-BN sheet results in only one independent element for the piezoelectricity tensor,  $d_0 = d_{y,yy}$ . The tensor is invariant under a rotation angle of  $2\pi/3$  about the  $z$ -axis which yields the following symmetry relations:  $d_{y,yy} = -d_{y,xx} = -d_{x,yy} = -d_{x,xx}$ . Substituting  $\sigma(x, y)$  in Eq. (1) results in the local induced dipoles:

$$P_x = -8d_0 \mu C x, \quad P_y = -8d_0 \mu C y. \quad (1)$$

Note that the local dipoles are directed radially inward, i.e.  $P = -8d_0 \mu C r \vec{e}_r$  with magnitude  $8d_0 \mu C$  per unit of radial distance. For a disk with diameter  $D = 2R$  and using  $C = \delta/D$ , the total induced dipole moment is found to be zero by integrating over the disk from 0 to  $\phi$

$$P_x^T = -2d_0 \mu \delta R \sin(\phi), P_y^T = +2d_0 \mu \delta R \cos(\phi), \quad (2)$$

where  $\phi = 2\pi$  i.e.  $P_x^T(2\pi) = P_y^T(2\pi) = 0$ . Notice that  $P_i^T(\pi) = P_i^T(-\pi)$ . The local  $P$  results in a surface charge density ( $\sigma_p = -\nabla \cdot P$ ) and a boundary charge density ( $\lambda_p = -P \cdot \vec{e}_r$ ), hence the corresponding electrostatic potential  $\phi_P(\vec{x})$  which is proportional to  $\int \frac{\sigma_p ds'}{|\vec{x} - \vec{x}'|} + \oint \frac{\lambda_p dl'}{|\vec{x} - \vec{x}'|}$  can be written in terms of Bessel functions of the second kind and results in a radially decreasing potential. For a disk with radius  $R$ , the first integral is taken over the disk surface and the second

is taken over its perimeter. In 2 we show  $\phi_P(\vec{x})$  in x-y plane at height  $z = 2 \times 10^{-4}R$  above a circular flake with radius  $R$ . These results are in qualitative agreement with the electrostatic potential (ESP) obtained from our DFT results shown in 4(a,d). Notice that for uniaxial strain, e.g.  $u = (x, 0)$  and shear strain, e.g.  $u = (y, x)$  the used formalism gives  $P = (P_x, 0) = (\mu d_0, 0)$  and  $P = (0, P_y) = (0, -2\mu d_0)$ , respectively, which are in agreement with the DFT results of Ref.<sup>12</sup> It is important to note that the above model is size-independent and is valid also for an infinitely large h-BN flake. On the other hand applying strain on the N-edges (NB-system) is equivalent to the transformation  $\theta \rightarrow \theta + \pi/3$  in  $u$  which yields  $u_{NB} = -Cr^2(\sin(3\theta), \cos(3\theta))$ . Rewriting the above theory for the latter displacement vector results in  $P = 8d_0\mu Cr\vec{e}_r$  which has the opposite direction of the dipole moment of BN. This is in agreement with our DFT results shown in 4(d,e,f) for NB (we will discuss our DFT results below). We conclude that for an infinite hexagonal flake with zig-zag edges we have the opposite localization scheme for HOMO and LUMO depending on whether strain is applied on the N-edges or the B-edges.

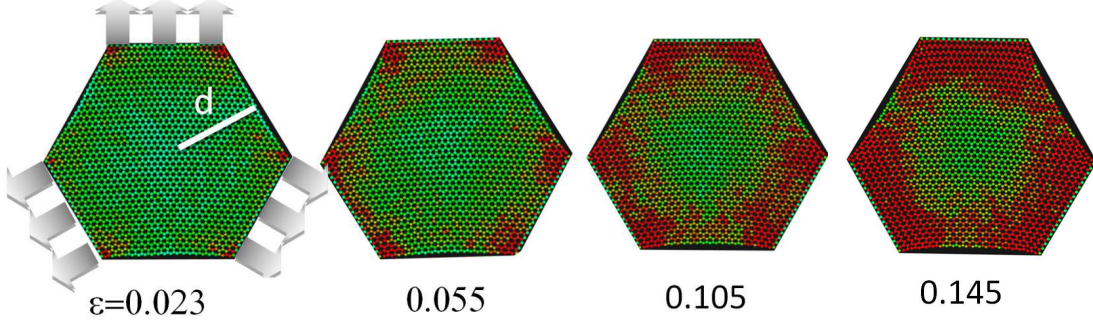


Figure 3: Four representative snapshots of molecular dynamics simulations of the hexagonal shaped h-BN flake subject to triaxial strain. The red and blue colors indicate the regions with highest and lowest stress, respectively. The direction of the applied strain  $\epsilon$  is shown by the arrows in the first snapshot and  $d=4.6$  nm.

## Computational Details

First, in order to study the stress distribution<sup>28</sup> on a large scale h-BN flake, we performed classical molecular dynamics (MD) simulation at  $T=300$  K for a system with 2400 atoms. We used a



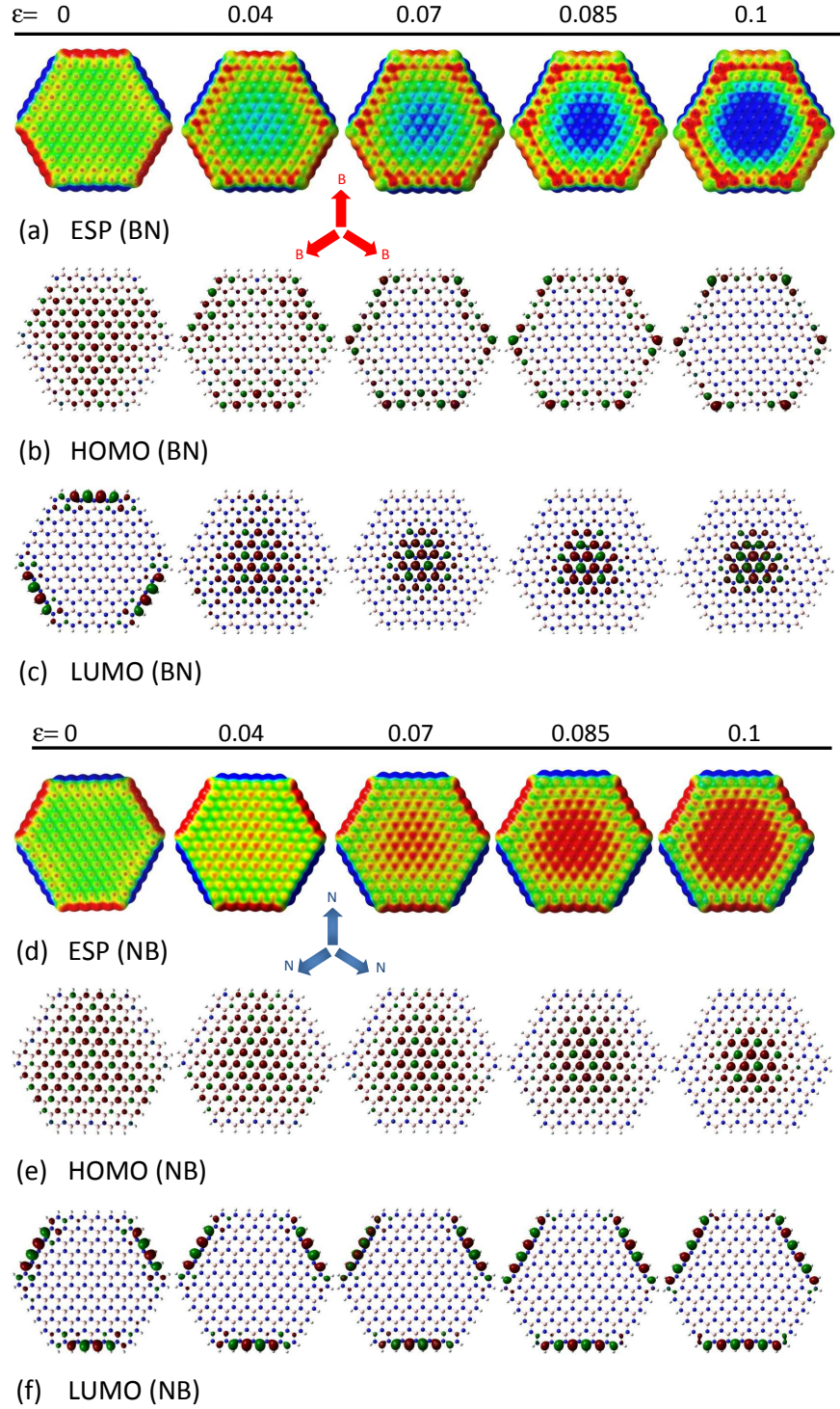


Figure 4: (a,d) Electrostatic potential surface mapped on an isosurface of electronic density of  $1.5 \times 10^{-2} \text{ e}/\text{\AA}^3$ , (b,e) highest occupied and (c,f) lowest unoccupied molecular orbitals for hexagonal shaped h-BN flakes subject to different triaxial strains  $\epsilon$  applied along the directions indicated by the arrows. The lower (higher) ESP is indicated by red (blue) color. In BN system (a, b, c) the stretched edges are terminated by B atoms while in NB system (d, e, f) the edges terminated by N atoms are stretched. Note that rotating the  $\epsilon = 0$  panels in (a,b,c) by an angle  $\pi/3$  gives the  $\epsilon = 0$  panels in (d,e,f), respectively.

modified Tersoff potential (which is defined in the LAMMPS package<sup>29,30</sup>) using the parameters proposed by Sevik *et al*<sup>31,32</sup> for a h-BN sheet. 3 shows four snapshots of our MD simulation for a h-BN flake with three of the zig-zag edges subject to triaxial strain as shown by the arrows. Notice that the corners are always under higher stress (red color) while the central atoms are subject to a reduced stress (blue color) (this results in a high pseudomagnetic field at the corners in case of graphene<sup>2</sup>).

To study the electronic behavior of the flakes in response to triaxial strain, we employ DFT as implemented in the GAUSSIAN (G09) package.<sup>33</sup> The electronic wavefunction is expanded using the 6-31G\* Gaussian type basis set and the exchange-correlation is treated using the hybrid functional B3LYP. The self consistency loop iterates until the change in the total energy is less than  $10^{-7}$  eV. In an unstrained hexagonal flake, distance of the edges to the center is denoted by  $d_0$ . The triaxial strain ( $\varepsilon = \delta/d_0$ ) is applied stepwise by rigidly displacing the atoms on the edges in directions normal to the corresponding edges such that the distance of the edges from the center becomes  $d = d_0 + \delta$ . Note that all atoms on each zig-zag edge are of the same type (see 1).

## Results and Discussion

In order to explain the change in the main electronic properties as resulting from triaxial strain in BN and NB flakes one should consider the following issues: i) contrary to the fixed edges, the free edges are relaxed (hence can expand) when applying strain; ii) as we showed in section II both BN and NB under stress become polarized locally with different orientation while the total dipole moment is zero, iii) the polarization and the electrostatic potential distribution in the system correlate, and iv) all edges (both BN and NB) are passivated by hydrogens and because of the difference of electronegativity of H, B and N the results will be different for unsaturated flake edges.

## Localized states and electrostatic potential

The electrostatic potential, highest occupied and lowest unoccupied molecular orbitals obtained from the DFT calculations for a hexagonal shaped h-BN flake consisting of 252 atoms ( $d_0 = 1.35$  nm) are shown in 4 for five different values of  $\varepsilon = \delta/d_0$ . When the flake is stretched at the B edges (i.e. BN system, 4(a-c)), both the region with higher ESP and the LUMO are localized in the central part. On the other hand, when strain is applied on the N edges (i.e. NB system, 4(d-f)), the region with lower ESP and the HOMO both are localized again in the center. In the unstrained ( $\varepsilon=0$ ) flakes the LUMO is localized on the N-edges, while the HOMO is not concentrated on the B-edges which is different from the case of rectangular ribbons.<sup>16,34</sup> For a rectangular ribbon the N atoms absorb electrons from H and therefore the HOMO is localized on the N atoms while in the B edges the H atoms gain electronic charge from those B atoms and the B atoms lose their electrons and consequently the LUMO is on the B atoms. In the hexagonal unstrained flakes, the N atoms absorb electrons and the HOMO is also on the N atoms. But the LUMO is only on the B atoms in the mid point of the B edge while the B atoms situated at the corners of the B edge do not contribute in the LUMO. The reason is that the corner B atoms recover their lost electrons from their N neighbors at the same corner. In 5(a) the Mulliken charge change when applying 10% strain is shown for a BN flake with 432 atoms. It is seen that the B atoms transfer electrons to N atoms which make the system highly polarized. The charge distribution reveals the corresponding triaxial applied stress shown in 1(b).

The larger  $\varepsilon$ , the more localized the HOMO (LUMO) in the center of the NB (BN) flake. This is due to the appearance of longer bond-lengths ( $a_{BN}$ ). The longer the B-N bond length, there is the less  $2p_z$  hybridization. In 5(b) the distribution of  $a_{BN}$  for a strained BN flake ( $\varepsilon = 10\%$ ) is shown (bonds longer than  $1.6 \text{ \AA}$  are not shown for clarity). This bond length distribution shows the weakening of the covalent bond perpendicular to the stressed edges. One can connect this pattern to those shown in 4(a,b,c). The longer the bonds perpendicular to the B (N) edge in a BN (NB) flake the larger the inward (outward) dipole moment.

The gradient in ESP from the edges into the center increases with increasing  $\varepsilon$ . We performed

also DFT calculations to study similar effects in a graphene flake with the same size but no such localization/polarization effects were found.

In order to ensure that the observed effect is independent of the flake size, we performed calculations<sup>35,36</sup> for a larger flake with 2520 atoms ( $d_0 = 4.6$  nm) and found similar localized frontier orbitals as shown in 6. The reason for the specific spatial localization of the frontier orbitals is the rehybridization of the electronic orbitals due to the new position of the atoms. The induced inhomogeneous strain changes the bonds non-uniformly and yields local dipoles which are mainly oriented radially. Note that in general, finite flakes or nanoribbons of h-BN might be polarized due to their finite size.<sup>16</sup> However, here the finite flake has zero total dipole moment because of the symmetry of the flake even when it is subject to triaxial strain.

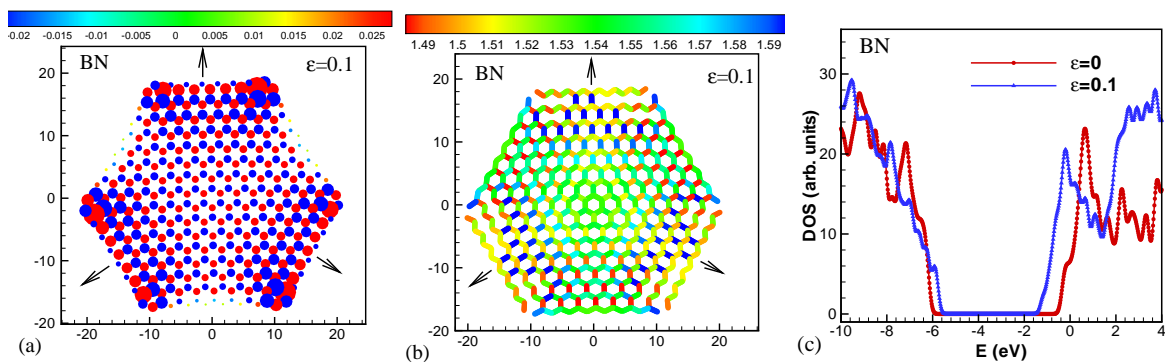


Figure 5: (a) The Change in the Mulliken charges induced by applying strain ( $\epsilon = 10\%$ ) to the BN flake. Circle radius corresponds to the charge difference between strained and unstrained BN flakes. (b) The bond length, i.e.  $a_{BN}$ , distribution in a strained BN flake ( $\epsilon = 10\%$ ). For clarity, bonds longer than  $1.6 \text{ \AA}$  are not shown. (c) DOS spectra of strained (10%) and unstrained BN flakes.

## Strain energy and gap variation

7(a) shows the variation of the strain energy as function of the applied strain which exhibits a quadratic behavior as expected from Hooke's law. 7(b) shows the variation of the HOMO-LUMO energy gap with  $\epsilon$ . The density of states (DOS) spectra for strained ( $\epsilon = 10\%$ ) and unstrained BN flakes are shown in 5(c). By applying the strain, the HOMO-LUMO gap decreases by about 2 eV,

and new peaks appear above the LUMO. The decreasing of the gap and modification of the DOS profile with increasing strain is attributed to the spatial localization of the HOMO and LUMO on regions with different ESP. For example, applying strain on the BN flake localizes the LUMO at the center of the flake where the electrostatic energy of an electron is lower because of high ESP. Similarly, applying strain on the NB flake rises its HOMO energy level because it localizes the HOMO at the center where ESP is lower in this case. For larger strains the energy difference of the localized states at the center and the edges becomes larger resulting in a smaller energy difference of the frontier orbitals, i.e. smaller gap. The different dependence of the gap on the strain for BN and NB (see 7(b)) is a consequence of the distributed HOMO along all the edges and mostly the corners of the strained BN system and the fact that the LUMO is localized at the B edges in the NB system. Similar effect has been seen by applying an external electric field to nanoribbons.<sup>16</sup> Note that the strain induced change in the conductance of graphene was previously investigated<sup>2,37</sup> but at present no similar study is available yet for h-BN.

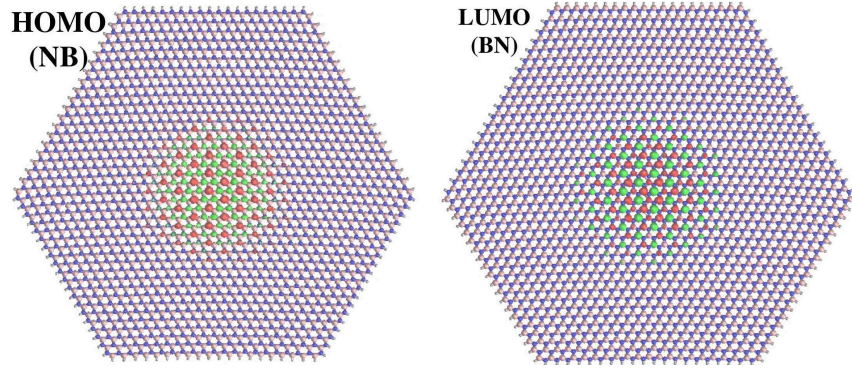


Figure 6: HOMO of NB (left) and LUMO of BN (right) flakes with 2520 atoms ( $d_0 = 4.6$  nm) subjected to the strain  $\epsilon = 0.15$ . Notice that for this larger system we can apply larger strain as compared to the smaller system shown in Figure 4.

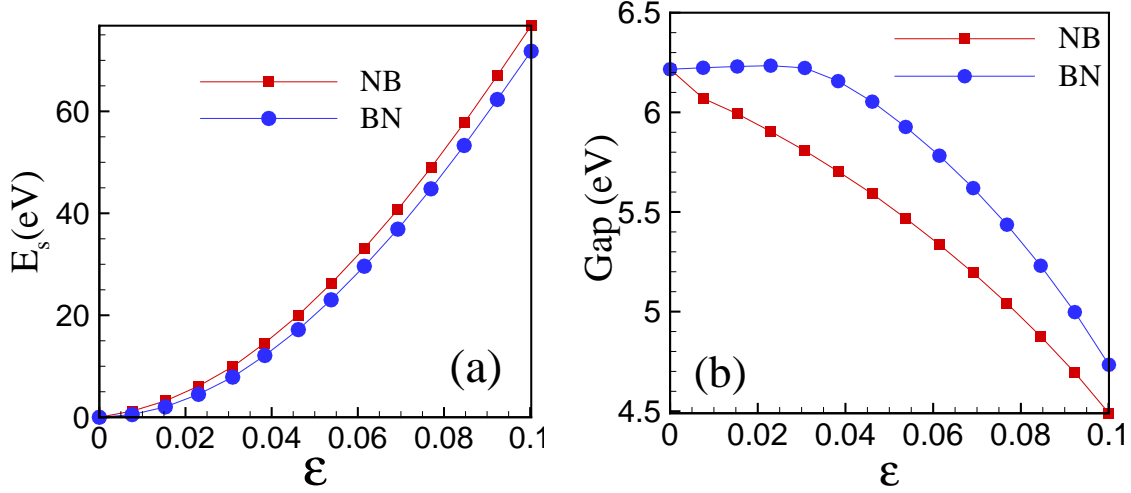


Figure 7: (a) The strain energy of the hexagonal shaped BN and NB flakes as function of the strain parameter, i.e.  $\epsilon$ . (b) The variation of the energy gap with  $\epsilon$ . Each flake consists of 252 atoms.

## Application as a gas nanosensor

Two alternative methods to realize this kind of triaxial stretching of two dimensional materials<sup>1,2</sup> are proposed recently. It was reported experimentally<sup>1</sup> that nanobubbles of graphene grown on a Pt(111) surface suffice very high inhomogeneous triaxial strain which changes significantly the electronic properties of graphene resulting in e.g. a pseudo-magnetic fields larger than 300 Tesla. The following experimental set up might also be possible: Fixing the 2D layer (here h-BN) on a triangular shaped trench and subsequently injecting a high pressure gas into the hole will stretch the 2D layer and exerts a triaxial inhomogeneous strain on the flake.

The controllable localizing of the frontier orbitals in the central part of the h-BN flake is important for nanosensing technological applications, e.g. for filtering gas adsorbates. The key idea is to control the binding energy of a molecule, namely

$$E_b = (E_{molecule} + E_{flake}) - E_{molecule/flake} \quad (3)$$

via the applied strain. Here  $E_{molecule}$  and  $E_{flake}$  are the energies of the pristine molecule and flake,



respectively, while  $E_{molecule/flake}$  is the energy of the molecule over the examined flake. As an example, we study here the adsorption of an ammonia molecule as function of the strain on the h-BN flake. We put the  $\text{NH}_3$  molecule in the central region of the stretched flake and relax the system under external triaxial strain. Starting from different orientations, we found the minimum energy when the molecule is adsorbed onto a B atom in the middle as shown in 8(a,b). More importantly, as seen in 8(c), the binding energy depends strongly on the strain such that by applying a strain of 10% the binding energy is almost doubled. One notes that  $\epsilon = 0$  indeed gives the minimal  $E_b$ . We performed similar calculations when the flake is triaxially compressed and found that the binding energy also increases.

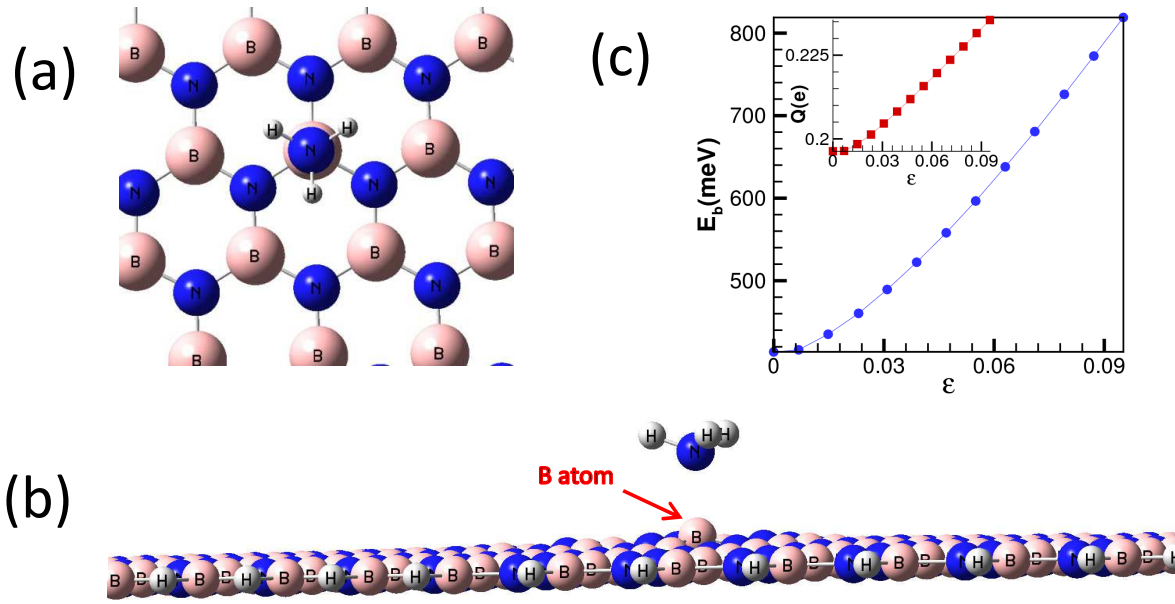


Figure 8: Top (a) and side (b) view of the adsorbed  $\text{NH}_3$  on a h-BN hexagonal flake. (c) The variation of the binding energy and Mulliken charge on the  $\text{NH}_3$  molecule (inset) vs the strain.

$\text{NH}_3$  has one lone pair of electrons on the nitrogen atom making it an electron donor. Therefore the molecule is positively charged when chemically bonded to the B atom. 9(a) depicts the electron density mapped on the plane containing this B-N bond when the flake is not stretched. The impact of strain on the redistribution of the electronic charge is seen in 9(b) and it predicts a stronger covalent bonding between the molecule and the flake. Consistently, the total Mulliken charge on

$\text{NH}_3$  increases monotonically from 0.19 e for the unstrained flake to 0.23 e when  $\varepsilon = 0.1$ . In the same time, the binding energy increases from 0.41 eV to 0.82 eV as shown in 8(c). Triaxially stretching the flake also quenches its buckling due to the interaction with the adsorbed molecule such that the out of plane height of the B atom under the ammonia molecule is 0.68 and 0.34 Å for zero and  $\varepsilon = 0.1$  strains, respectively. Finally, the length of the chemical bond between the N atom of  $\text{NH}_3$  and the B atom of the flake also decreases monotonically from 1.83 to 1.75 Å between the mentioned strains. Notice that, the binding energy of the  $\text{NH}_3$  molecule is almost the same on any B atom in the region around the center of the BN system where the LUMO is extended.

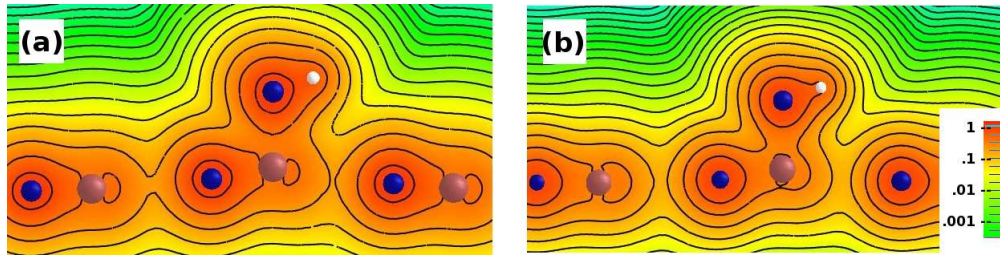


Figure 9: Contour maps of the electron density around the chemical bond between an ammonia molecule and a central B atom of a BN flake subject to zero (a) and  $\varepsilon = 0.1$  (b) strain. The plane of the map is normal to the flake and passes through N and one of the H atoms of  $\text{NH}_3$ . We put N in blue, B in purple and H in white (c.f. 8(a)). The successive contours differ by  $10^{1/4}$  and the color bar shows the electron density in atomic units.

The enhancement of the adsorption of  $\text{NH}_3$  on the BN flake by strain can be explained in the framework of the so-called frontier molecular orbitals theory<sup>38</sup> which implies that there is a higher tendency for adsorption of such a molecule onto those sites of the flake where the LUMO is localized, i.e. the central part. However, for the NB flake the central part has no contribution to the LUMO and we found that the binding energy is more than twice smaller than for the BN flake.

## Conclusions

In summary, by using DFT calculations we showed that the occupied (unoccupied) orbitals of a hexagonal shaped h-BN flake can be localized in the center of the flake by applying triaxial strain



on the N(B) atoms at the edges of the sample. The h-BN flake is locally polarized but the net polarization is zero. As an example we investigated the adsorption of ammonia and found its adsorption on the B-edges stretched BN flake is more likely than on the N-edges stretched flake. This is a consequence of the specific spatial localization of the frontier orbitals. This particular kind of localization of the frontier orbitals might have technological applications for the design of piezoelectric and nanosensor devices.

## Acknowledgement

This work was supported by the EU-Marie Curie IIF postdoc Fellowship/299855 (for M.N.-A.), the ESF EuroGRAPHENE project CONGRAN, the Flemish Science Foundation (FWO-VI) and the Methusalem Funding of the Flemish government. A. S. would like to thank the Universiteit Antwerpen for its hospitality.

## References

- (1) Levy, N.; Burke, S.; Meaker, K.; Panlasigui, M.; Zettl, A.; Guinea, F.; Neto, A. C.; Crommie, M. Strain-Induced Pseudo-Magnetic Fields Greater Than 300 Tesla in Graphene Nanobubbles. *Science* **2010**, *329*, 544–547.
- (2) Guinea, F.; Katsnelson, M.; Geim, A. Energy Gaps and a Zero-Field Quantum Hall Effect in Graphene by Strain Engineering. *Nat. Phys.* **2009**, *6*, 30–33.
- (3) Blase, X.; Rubio, A.; Louie, S. G.; Cohen, M. L. Quasiparticle Band Structure Of Bulk Hexagonal Boron Nitride And Related Systems. *Phys. Rev. B* **1995**, *51*, 6868–6868.
- (4) Watanabe, K.; Taniguchi, T.; Kanda, H. Direct-Bandgap Properties and Evidence for Ultra-violet Lasing of Hexagonal Boron Nitride Single Crystal. *Nat. Mater.* **2004**, *3*, 404–409.
- (5) Pacilé, D.; Meyer, J. C.; Girit, Ç. Ö.; Zettl, A. The Two-dimensional Phase of Boron Nitride:

- few-atomic-layer Sheets and Suspended Membranes. *Appl. Phys. Lett.* **2008**, *92*, 133107–133107.
- (6) Britnell, L.; Gorbachev, R. V.; Jalil, R.; Belle, B. D.; Schedin, F.; Katsnelson, M. I.; Eaves, L.; Morozov, S. V.; Mayorov, A. S.; Peres, N. M. R.; et al. Electron Tunneling Through Ultrathin Boron Nitride Crystalline Barriers. *Nano Lett.* **2012**, *12*, 1707–1710.
  - (7) Alem, N.; Erni, R.; Kisielowski, C.; Rossell, M. D.; Gannett, W.; Zettl, A. Atomically Thin Hexagonal Boron Nitride Probed by Ultrahigh-resolution Transmission Electron Microscopy. *Phys. Rev. B* **2009**, *80*, 155425–155425.
  - (8) Zheng, F.; Zhou, G.; Liu, Z.; Wu, J.; Duan, W.; Gu, B.-L.; Zhang, S. Half Metallicity Along the Edge of Zigzag Boron Nitride Nanoribbons. *Phys. Rev. B* **2008**, *78*, 205415–205415.
  - (9) Wang, Y.; Ding, Y.; Ni, J. Fluorination-Induced Half-metallicity In Zigzag Boron Nitride Nanoribbons: First-principles Calculations. *Phys. Rev. B* **2010**, *81*, 193407–193407.
  - (10) Ding, Y.; Wang, Y.; Ni, J. The Stabilities of Boron Nitride Nanoribbons with Different Hydrogen-terminated Edges. *Appl. Phys. Lett.* **2009**, *94*, 233107–233107.
  - (11) Michel, K. H.; Verberck, B. Phonon Dispersions and Piezoelectricity in Bulk and Multilayers Of Hexagonal Boron Nitride. *Phys. Rev. B* **2011**, *83*, 115328–115328.
  - (12) Sai, N.; Mele, E. Microscopic Theory for Nanotube Piezoelectricity. *Phys. Rev. B* **2003**, *68*, 241405–241405.
  - (13) Naumov, I.; Bratkovsky, A. M.; Ranjan, V. Unusual Flexoelectric Effect in Two-Dimensional Noncentrosymmetric  $sp^2$ -Bonded Crystals. *Phys. Rev. Lett.* **2009**, *102*, 217601.
  - (14) Peng, Q.; Ji, W.; De, S. Mechanical Properties of The Hexagonal Boron Nitride Monolayer: Ab Initio Study. *Comp. Mater. Sci.* **2012**, *56*, 11–17.
  - (15) Peng, Q.; Zamiri, A. R.; Ji, W.; De, S. Elastic Properties of Hybrid Graphene/boron Nitride Monolayer. *Acta Mechanica* **2012**, *223*, 2591–2596.

- (16) Beheshtian, J.; Sadeghi, A.; Neek-Amal, M.; Michel, K.; Peeters, F. Induced Polarization And Electronic Properties of Carbon-Doped Boron Nitride Nanoribbons. *Phys. Rev. B* **2012**, *86*, 195433–195433.
- (17) Khoo, K. H.; Mazzoni, M. S. C.; Louie, S. G. Tuning The Electronic Properties Of Boron Nitride Nanotubes With Transverse Electric Fields: A Giant dc Stark Effect. *Phys. Rev. B* **2004**, *69*, 201401–201401.
- (18) Park, C.-H.; Louie, S. G. Energy Gaps and Stark Effect in Boron Nitride Nanoribbons. *Nano Lett.* **2008**, *8*, 2200–2203.
- (19) Ishigami, M.; Sau, J. D.; Aloni, S.; Cohen, M. L.; Zettl, A. Observation of the Giant Stark Effect in Boron-Nitride Nanotubes. *Phys. Rev. Lett.* **2005**, *94*, 056804–056804.
- (20) Hu, M.; Yu, Z.; Zhang, K.; Sun, L.; Zhong, J. Tunneling Magnetoresistance of Bilayer Hexagonal Boron Nitride and Its Linear Response to External Uniaxial Strain. *J. Phys. Chem. C* **2011**, *115*, 8260–8264.
- (21) Collins, P. G.; Zettl, A.; Bando, H.; Thess, A.; Smalley, R. Nanotube Nanodevice. *Science* **1997**, *278*, 100–102.
- (22) 287, 1801–1804.
- (23) Kong, J.; Franklin, N. R.; Zhou, C.; Chapline, M. G.; Peng, S.; Cho, K.; Dai, H. Nanotube Molecular Wires as Chemical Sensors. *Science* **2000**, *287*, 622–625.
- (24) Di Francia, G.; Alfano, B.; La Ferrara, V. Conductometric Gas Nanosensors. *J. Sensors* **2009**, *2009*, 659275–659275.
- (25) Jia, X.; Hofmann, M.; Meunier, V.; Sumpter, B. G.; Campos-Delgado, J.; Romo-Herrera, J. M.; Son, H.; Hsieh, Y.-P.; Reina, A.; Kong, J.; et al. Controlled Formation of Sharp Zigzag and Armchair Edges in Graphitic Nanoribbons. *Science* **2009**, *323*, 1701–1705.

- (26) Hämäläinen, S. K.; Sun, Z.; Boneschanscher, M. P.; Uppstu, A.; Ijäs, M.; Harju, A.; Vanmaekelbergh, D.; Liljeroth, P. Quantum-Confined Electronic States in Atomically Well-Defined Graphene Nanostructures. *Phys. Rev. Lett.* **2011**, *107*, 236803–236803.
- (27) Begliarbekov, M.; Sasaki, K.-I.; Sul, O.; Yang, E.-H.; Strauf, S. Optical Control of Edge Chirality in Graphene. *Nano Lett.* **2011**, *11*, 4874–4878.
- (28) Neek-Amal, M.; Covaci, L.; Peeters, F. M. Nanoengineered Nonuniform Strain in Graphene Using Nanopillars. *Phys. Rev. B* **2012**, *86*, 041405–041405.
- (29) <http://lammmps.sandia.gov>.
- (30) Plimpton, S. Fast Parallel Algorithms for Short-range Molecular Dynamics. *J. Comp. Phys.* **1995**, *117*, 1–19.
- (31) Sevik, C.; Kinaci, A.; Haskins, J. B.; Çağın, T. Characterization of Thermal Transport in Low-Dimensional Boron Nitride Nanostructures. *Phys. Rev. B* **2011**, *84*, 085409–085409.
- (32) Singh, S. K.; Neek-Amal, M.; Costamagna, S.; Peeters, F. M. Thermomechanical Properties of a Single Hexagonal Boron Nitride Sheet. *Phys. Rev. B* **2013**, *87*, 184106–184106.
- (33) Frisch, M. J.; Trucks, G. W.; Schlegel, H. B.; Scuseria, G. E.; Robb, M. A.; Cheeseman, J. R.; Scalmani, G.; Barone, V.; Mennucci, B.; Petersson, G. A.; et al. *Gaussian 09 Revision A.1*, Gaussian Inc. Wallingford CT 2009.
- (34) Nakamura, J.; Nitta, T.; Natori, A. Electronic and Magnetic Properties of BNC Ribbons. *Phys. Rev. B* **2005**, *72*, 205429–205429.
- (35) Aradi, B.; Hourahine, B.; Frauenheim, T. DFTB+, A Sparse Matrix-based Implementation of The DFTB Method. *J. Phys. Chem. A* **2007**, *111*, 5678–5684.
- (36) Lukose, B.; Kuc, A.; Frenzel, J.; Heine, T. On The Reticular Construction Concept of Covalent Organic Frameworks. *Beilstein J. Nanotech.* **2010**, *1*, 60–70.

- (37) Teague, M.; Lai, A.; Velasco, J.; Hughes, C.; Beyer, A.; Bockrath, M.; Lau, C.; Yeh, N.-C. Evidence for Strain-induced Local Conductance Modulations in Single-layer Graphene on SiO<sub>2</sub>. *Nano Lett.* **2009**, 9, 2542–2546.
- (38) Fukui, K.; Yonezawa, T.; Shingu, H. A Molecular Orbital Theory of Reactivity in Aromatic Hydrocarbons. *J. Chem. Phys.* **1952**, 20, 722–725.

## Table of Contents Image

